A new hybrid gadolinium nanoparticles-loaded polymeric material for neutron detection in rare event searches

F. Acerbi[1] P. Adhikari[2] P. Agnes[3,4] I. Ahmad[5] S. Albergo[6,7] I. F. Albuquerque[8]
T. Alexander[9] A. K. Alton[10] P. Amaudruz[11] M. Angiolilli[3,4] E. Aprile[12] R. Ardito[13,14]
M. Atzori Corona[15,16] D. J. Auty[17] M. Ave[8] I. C. Avetisov[18] O. Azzolini[19] H. O. Back[20]
Z. Balmforth[21] A. Barrado Olmedo[22] P. Barrillon[23] G. Batignani[24,25] P. Bhowmick[26]
V. Bocci[27] W. Bonivento[15] B. Bottino[28,29] M. G. Boulay[2] A. Buchowicz[30] S. Bussino[31]
J. Busto[23] M. Cadeddu[15] M. Cadoni[15,16] R. Calabrese[32] V. Camillo[33] A. Caminata[29]
N. Canci[32] A. Capra[11] M. Caravati[3,4] M. Cárdenas-Montes[22] N. Cargioli[15,16] M. Carlini[4]
A. Castellani[13,14] P. Castello[15,55] P. Cavalcante[4] D. Cavallo[82,29] S. Cebrian[34] J. Cela Ruiz[22]
S. Chashin[35] A. Chepurnov[35] L. Cifarelli[36,37] D. Cintas[34] M. Citterio[14] B. Cleveland[38,39]
Y. Coadou[23] V. Cocco[15] D. Colaiuda[4,56] E. Conde Vilda[22] L. Consiglio[4] B. S. Costa[8]
M. Czubak[40] M. D'Aniello[32,83] S. D'Auria[14,75] M. D. Da Rocha Rolo[41] G. Darbo[29] S. Davini[29]
S. De Cecco[44,27] G. De Guido[14,76] G. Dellacasa[41] A. V. Derbin[42] A. Devoto[15,16] F. Di
Capua[49,32] A. Di Ludovico[4] L. Di Noto[29] P. Di Stefano[43] L. K. Dias[8] D. Díaz Mairena[22]
X. Ding[45] C. Dionisi[44,27] G. Dolganov[46] F. Dordei[15] V. Dronik[47] A. Elersich[48]
E. Ellingwood[43] T. Erjavec[48] M. Fernandez Diaz[22] A. Ficorella[1] G. Fiorillo[49,32]
P. Franchini[21,51] D. Franco[52] H. Frandini Gatti[53] E. Frolov[54] F. Gabriele[15] D. Gahan[15,16]
C. Galbiati[45] G. Galiński[30] G. Gallina[45] G. Gallus[15,55] M. Garbini[57,37] P. Garcia Abia[22]
A. Gawdzik[58] A. Gendotti[59] A. Ghisi[13,14] G. K. Giovanetti[60] V. Goicoechea Casanueva[61]
A. Gola[1] L. Grandi[62] G. Grauso[32] G. Grilli di Cortona[4] A. Grobov[46] M. Gromov[35]
M. Guerzoni[37] M. Gulino[63] C. Guo[64] B. R. Hackett[9] A. Hallin[17] A. Hamer[65] M. Haranczyk[40]
B. Harrop[45] T. Hessel[52] S. Hill[21] S. Horikawa[4,56] J. Hu[17] F. Hubaut[23] J. Hucker[43]
T. Hugues[43] E. V. Hungerford[66] A. Ianni[45] V. Ippolito[27] A. Jamil[45] C. Jillings[38,39]
P. Kachru[3,4] R. Keloth[33] N. Kemmerich[8] A. Kemp[26] C. L. Kendziora[45] M. Kimura[5]
K. Kondo[4,56] G. Korga[21] L. Kotsiopoulou[65] S. Koulosousas[21] A. Kubankin[47] P. Kunzé[3,4]
M. Kuss[25] M. Kuźniak[5] M. Kuzwa[5] M. La Commara[32,50] M. Lai[67] E. Le Guirriec[23]
E. Leason[21] A. Leoni[4,56] L. Lidey[9] M. Lissia[15] L. Luzzi[22] O. Lychagina[68] O. Macfadyen[21]
I. N. Machulin[46,69] S. Manecki[38,39,43] I. Manthos[70,71] L. Mapelli[45] A. Marasciulli[4]
S. M. Mari[31] C. Mariani[33] J. Maricic[61] A. Marini[29] M. Martinez[34] C. J. Martoff[9,84]
G. Matteucci[49,32] K. Mavrokoridis[53] A. B. McDonald[43] J. Mclaughlin[21,11] S. Merzi[1]
A. Messina[44,27] R. Milincic[61] S. Minutoli[29] A. Mitra[72] A. Moharana[3,4] S. Moioli[14,76]
J. Monroe[26] E. Moretti[1] M. Morrocchi[24,25] T. Mroz[40] V. N. Muratova[42] M. Murphy[33]
M. Murra[12] C. Muscas[15,55] P. Musico[29] R. Nania[37] M. Nessi[73] G. Nieradka[5]
K. Nikolopoulos[70,71] E. Nikoloudaki[52] J. Nowak[51] K. Olchanski[11] A. Oleinik[47]

V. Oleynikov[54] P. Organtini[4,45] A. Ortiz de Solórzano[34] M. Pallavicini[28,29] L. Pandola[63]

E. Pantic[48] E. Paoloni[24,25] D. Papi[17] G. Pastuszak[30] G. Paternoster[1] D. Peddis[82,29]

P. A. Pegoraro[15,55] K. Pelczar[40] L. A. Pellegrini[14,76] R. Perez[8] F. Perotti[13,14] V. Pesudo[22]

S. I. Piacentini[44,27] N. Pino[7,6] G. Plante[12] A. Pocar[74] M. Poehlmann[48] S. Pordes[33]

P. Pralavorio[23] D. Price[58] S. Puglia[6,7] M. Queiroga Bazetto[53] F. Ragusa[14,75]

Y. Ramachers[72] A. Ramirez[66] S. Ravinthiran[53] M. Razeti[15] A. L. Renshaw[66] M. Rescigno[27]

F. Retiere[11] L. P. Rignanese[37] A. Rivetti[41] A. Roberts[53] C. Roberts[58] G. Rogers[70]

L. Romero[22] M. Rossi[29] A. Rubbia[59] D. Rudik[49,32,69] M. Sabia[44,27] S. Sadashivajois[21]

P. Salomone[44,27] O. Samoylov[68] E. Sandford[58] S. Sanfilippo[63] D. Santone[21]

R. Santorelli[22] E. M. Santos[8] C. Savarese[58] E. Scapparone[37] G. Schillaci[63]

F. G. Schuckman II[43] G. Scioli[36,37] D. A. Semenov[42] A. Sheshukov[68] M. Simeone[85,32]

P. Skensved[43] M. D. Skorokhvatov[46,69] S. Slimani[82,29] O. Smirnov[68] T. Smirnova[46]

B. Smith[11] A. Sotnikov[68] F. Spadoni[9] M. Spangenberg[72] R. Stefanizzi[15] A. Steri[15,77]

V. Stornelli[4,56] S. Stracka[25] S. Sulis[15,55] A. Sung[45] C. Sunny[5] Y. Suvorov[49,32,46]

A. M. Szelc[65] O. Taborda[3,4] R. Tartaglia[4] A. Taylor[53] J. Taylor[53] S. Tedesco[41] G. Testera[29]

K. Thieme[61] A. Thompson[21] A. Tonazzo[52] S. Torres-Lara[66] S. Tosi[28,29] A. Tricomi[6,7]

E. V. Unzhakov[42] T. J. Vallivilayil[3,4] M. Van Uffelen[23] L. Velazquez-Fernandez[65] T. Viant[59]

S. Vicini[82,29] S. Viel[2] A. Vishneva[68] R. B. Vogelaar[33] J. Vossebeld[53] B. Vyas[2] M. Wada[5]

M. B. Walczak[3,4] H. Wang[78] Y. Wang[64,79] S. Westerdale[67] L. Williams[80] R. Wojaczyński[5]

M. M. Wojcik[40] M. Wojcik[81] T. Wright[33] Y. Xie[64,79] C. Yang[64,79] J. Yin[64,79] A. Zabihi[5]

P. Zakhary[5] A. Zani[14] Y. Zhang[64] T. Zhu[48] A. Zichichi[36,37] G. Zuzel[40] M. P. Zykova[18]

[1]*Fondazione Bruno Kessler, Povo 38123, Italy*

[2]*Department of Physics, Carleton University, Ottawa, ON K1S 5B6, Canada*

[3]*Gran Sasso Science Institute, L'Aquila 67100, Italy*

[4]*INFN Laboratori Nazionali del Gran Sasso, Assergi (AQ) 67100, Italy*

[5]*AstroCeNT, Nicolaus Copernicus Astronomical Center of the Polish Academy of Sciences, 00-614 Warsaw, Poland*

[6]*INFN Catania, Catania 95121, Italy*

[7]*Università of Catania, Catania 95124, Italy*

[8]*Instituto de Física, Universidade de São Paulo, São Paulo 05508-090, Brazil*

[9]*Pacific Northwest National Laboratory, Richland, WA 99352, USA*

[10]*Physics Department, Augustana University, Sioux Falls, SD 57197, USA*

[11]*TRIUMF, 4004 Wesbrook Mall, Vancouver, BC V6T 2A3, Canada*

[12]*Physics Department, Columbia University, New York, NY 10027, USA*

[13]*Civil and Environmental Engineering Department, Politecnico di Milano, Milano 20133, Italy*

[14]*INFN Milano, Milano 20133, Italy*

[15]*INFN Cagliari, Cagliari 09042, Italy*

[16]*Physics Department, Università degli Studi di Cagliari, Cagliari 09042, Italy*

[17]*Department of Physics, University of Alberta, Edmonton, AB T6G 2R3, Canada*

[18]*Mendeleev University of Chemical Technology, Moscow 125047, Russia*

[19]*INFN Laboratori Nazionali di Legnaro, Legnaro (Padova) 35020, Italy*

[20]*Savannah River National Laboratory, Jackson, SC 29831, United States*

[21]*Department of Physics, Royal Holloway University of London, Egham TW20 0EX, UK*

[22]*CIEMAT, Centro de Investigaciones Energéticas, Medioambientales y Tecnológicas, Madrid 28040, Spain*

[23]*Centre de Physique des Particules de Marseille, Aix Marseille Univ, CNRS/IN2P3, CPPM, Marseille, France*

[24]*Physics Department, Università degli Studi di Pisa, Pisa 56127, Italy*

[25]*INFN Pisa, Pisa 56127, Italy*

[26]*University of Oxford, Oxford OX1 2JD, United Kingdom*

[27]*INFN Sezione di Roma, Roma 00185, Italy*

[28]*Physics Department, Università degli Studi di Genova, Genova 16146, Italy*

[29]*INFN Genova, Genova 16146, Italy*

[30]*Institute of Radioelectronics and Multimedia Technology, Warsaw University of Technology, 00-661 Warsaw, Poland*

[31]*INFN Roma Tre, Roma 00146, Italy*

[32]*INFN Napoli, Napoli 80126, Italy*

[33]*Virginia Tech, Blacksburg, VA 24061, USA*

[34]*Centro de Astropartículas y Física de Altas Energías, Universidad de Zaragoza, Zaragoza 50009, Spain*

[35]*Skobeltsyn Institute of Nuclear Physics, Lomonosov Moscow State University, Moscow 119234, Russia*

[36]*Department of Physics and Astronomy, Università degli Studi di Bologna, Bologna 40126, Italy*

[37]*INFN Bologna, Bologna 40126, Italy*

[38]*Department of Physics and Astronomy, Laurentian University, Sudbury, ON P3E 2C6, Canada*

[39]*SNOLAB, Lively, ON P3Y 1N2, Canada*

[40]*M. Smoluchowski Institute of Physics, Jagiellonian University, 30-348 Krakow, Poland*

[41]*INFN Torino, Torino 10125, Italy*

[42]*Saint Petersburg Nuclear Physics Institute, Gatchina 188350, Russia*

[43]*Department of Physics, Engineering Physics and Astronomy, Queen's University, Kingston, ON K7L 3N6, Canada*

[44]*Physics Department, Sapienza Università di Roma, Roma 00185, Italy*

[45]*Physics Department, Princeton University, Princeton, NJ 08544, USA*

[46]*National Research Centre Kurchatov Institute, Moscow 123182, Russia*

[47]*Radiation Physics Laboratory, Belgorod National Research University, Belgorod 308007, Russia*

[48]*Department of Physics, University of California, Davis, CA 95616, USA*

[49]*Physics Department, Università degli Studi "Federico II" di Napoli, Napoli 80126, Italy*

[50]*Pharmacy Department, Università degli Studi "Federico II" di Napoli, Napoli 80131, Italy*

[51]*Physics Department, Lancaster University, Lancaster LA1 4YB, UK*

[52]*APC, Université de Paris, CNRS, Astroparticule et Cosmologie, Paris F-75013, France*

[53]*Department of Physics, University of Liverpool, The Oliver Lodge Laboratory, Liverpool L69 7ZE, UK*

[54]*Budker Institute of Nuclear Physics, Novosibirsk 630090, Russia*

[55]*Department of Electrical and Electronic Engineering, Università degli Studi di Cagliari, Cagliari 09123, Italy*

[56]*Università degli Studi dell'Aquila, L'Aquila 67100, Italy*

[57]*Museo Storico della Fisica e Centro Studi e Ricerche Enrico Fermi, Roma 00184, Italy*

[58]*Department of Physics and Astronomy, The University of Manchester, Manchester M13 9PL, UK*

[59]*Institute for Particle Physics, ETH Zürich, Zürich 8093, Switzerland*

[60]*Williams College, Physics Department, Williamstown, MA 01267 USA*

[61]*Department of Physics and Astronomy, University of Hawai'i, Honolulu, HI 96822, USA*

[62] *Department of Physics and Kavli Institute for Cosmological Physics, University of Chicago, Chicago, IL 60637, USA*

[63] *INFN Laboratori Nazionali del Sud, Catania 95123, Italy*

[64] *Institute of High Energy Physics, Chinese Academy of Sciences, Beijing 100049, China*

[65] *School of Physics and Astronomy, University of Edinburgh, Edinburgh EH9 3FD, UK*

[66] *Department of Physics, University of Houston, Houston, TX 77204, USA*

[67] *Department of Physics and Astronomy, University of California, Riverside, CA 92507, USA*

[68] *Joint Institute for Nuclear Research, Dubna 141980, Russia*

[69] *National Research Nuclear University MEPhI, Moscow 115409, Russia*

[70] *School of Physics and Astronomy, University of Birmingham, Edgbaston, B15 2TT, Birmingham, UK*

[71] *Institute of Experimental Physics, University of Hamburg, Luruper Chaussee 149, 22761, Hamburg, Germany*

[72] *University of Warwick, Department of Physics, Coventry CV47AL, UK*

[73] *Istituto Nazionale di Fisica Nucleare, Roma 00186, Italia*

[74] *Amherst Center for Fundamental Interactions and Physics Department, University of Massachusetts, Amherst, MA 01003, USA*

[75] *Physics Department, Università degli Studi di Milano, Milano 20133, Italy*

[76] *Chemistry, Materials and Chemical Engineering Department "G. Natta", Politecnico di Milano, Milano 20133, Italy*

[77] *Department of Mechanical, Chemical, and Materials Engineering, Università degli Studi, Cagliari 09042, Italy*

[78] *Physics and Astronomy Department, University of California, Los Angeles, CA 90095, USA*

[79] *University of Chinese Academy of Sciences, Beijing 100049, China*

[80] *Department of Physics and Engineering, Fort Lewis College, Durango, CO 81301, USA*

[81] *Institute of Applied Radiation Chemistry, Lodz University of Technology, 93-590 Lodz, Poland*

[82] *Chemistry and Industrial Chemistry Department, Università degli Studi di Genova, Genova 16146, Italy*

[83] *Department of Structures for Engineering and Architecture, Università degli Studi "Federico II" di Napoli, Napoli 80126, Italy*

[84] *Physics Department, Temple University, Philadelphia, PA 19122, USA*

[85] *Chemical, Materials, and Industrial Production Engineering Department, Università degli Studi "Federico II" di Napoli, Napoli 80126, Italy*

E-mail: bianca.bottino@ge.infn.it, anna.marini@ge.infn.it

ABSTRACT: Experiments aimed at direct searches for WIMP dark matter require highly effective reduction of backgrounds and control of any residual radioactive contamination. In particular, neutrons interacting with atomic nuclei represent an important class of backgrounds due to the expected similarity of a WIMP-nucleon interaction, so that such experiments often feature a dedicated neutron detector surrounding the active target volume. In the context of the development of DarkSide-20k detector at INFN Gran Sasso National Laboratory (LNGS), several R&D projects were conceived and developed for the creation of a new hybrid material rich in both hydrogen and gadolinium nuclei to be employed as an essential element of the neutron detector. Thanks to its very high cross-section for neutron capture, gadolinium is one of the most widely used elements in neutron detectors, while the hydrogen-rich material is instrumental in efficiently moderating the neutrons. In this paper results from one of the R&Ds are presented. In this effort the new hybrid material was obtained as a poly(methyl methacrylate) (PMMA) matrix, loaded with gadolinium oxide in the form of nanoparticles. We describe its realization, including all phases of design, purification, construction, characterization, and determination of mechanical properties of the new material.

Contents

1 Introduction

This paper describes one of the parallel R&D projects carried out by the DarkSide collaboration for the development of a new neutron-tagging material made of poly(methyl methacrylate), PMMA $(C_5O_2H_8)_n$, loaded with up to a few percent of gadolinium (Gd) by weight, referred to as Gd-PMMA in the following. This work has been driven by the requirements (Sec. 2) of DarkSide-20k (for a description of the detector see [1], an experiment aiming at the direct detection of WIMPs (Weakly Interacting Massive Particles) dark matter [2] at the Gran Sasso National Laboratory (LNGS), in

Italy. Since the low background level is one of the most important features for the experiment, as a first step we carried out extensive market research and screening of the radioactivity of the materials used in this R&D, in order to select the most suitable (Sec. 3). We have developed a method of production of Gd-PMMA with an extensive series of laboratory tests (Sec. 4) and we also set up and optimized a set of characterization measurements of the samples produced (Sec. 5). When the results obtained on laboratory samples were satisfactory, the process was transferred and adapted to industrial production (Sec. 6). The same procedures as developed during the laboratory test phase were used to perform the quality assurance of the industrially produced sheets.

The following considerations informed the development of the Gd-PMMA:

- the need for integration into the DarkSide-20k detector at LNGS, including operation in liquid argon at 87 K and full containment of Gd ensuring it can not be released into the environment;

- the need for a homogeneous distribution of gadolinium, of sufficient concentration, within the Gd-PMMA to ensure the neutron tagging is efficient throughout the detector;

- the need for minimal radioactivity of the product to keep the DarkSide-20k background within design limits, affecting the choice of primary ingredients and production procedures;

- the need to produce large quantities of Gd-PMMA, of the order of 20 t, using a Gd compound easily available on the market.

When appropriately coupled to standard commercial gamma-ray detectors, this material may be suitable for general purpose neutron detectors. Given its scalability and relatively low cost, our Gd-PMMA has excellent features for a neutron tagging material, not only for DarkSide-20k but also for other large detectors searching for rare events.

2   Requirements

2.1   Integration into DarkSide-20k

The center of the DarkSide-20k detector is a dual-phase liquid argon Time Projection Chamber (TPC) instrumented to detect scintillation photons produced in primary excitation of the argon and from electroluminescence produced by the ionization electrons in the gas region at the top of the TPC. The TPC is submerged in 100 t of low-radioactivity argon, extracted from underground sources. As demonstrated by the predecessor experiment DarkSide-50, in underground argon the level of the β-radioactive isotope ^{39}Ar is lower by more than a factor 1400 than in the standard argon of atmospheric origin [3–5]. The goal of the experiment is to observe WIMPs scattering elastically off the argon nucleus, whose recoil deposits tens to hundreds of keV of energy in the material. Fig. 1 shows a sketch of the DarkSide-20k detector with some details. The detector is designed for a 200 t·yr exposure with a negligible instrumental background level in the WIMP search region of interest. While argon has excellent rejection capabilities against electromagnetic backgrounds, neutrons with energy in the MeV range can produce an energy deposit in the TPC that mimics a WIMP signal. Nuclear recoils due to neutrons therefore must be efficiently identified and vetoed and this requires a detector to identify the neutron. The goal is to keep the neutron-induced
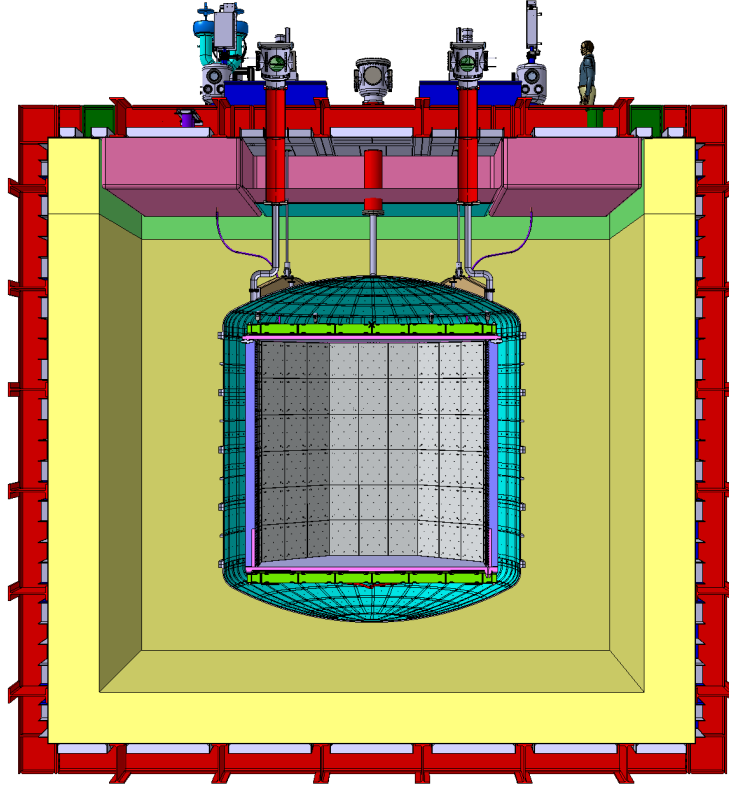
Figure 1: The picture shows a drawing of the DarkSide-20k apparatus. The innermost part is the TPC: the position of the Gd-PMMA lateral walls (which form an octagon) is shown in violet, while the pure PMMA windows at the top and bottom are depicted in pink. Above and below the pure PMMA windows there are the Gd-PMMA endcaps, which are represented in bright green. The TPC and Veto are contained in a stainless steel vessel, light blue in the picture, that holds the underground liquid argon. The vessel is hanging from the top of a big membrane cryostat (in red and yellow), that will be filled with atmospheric liquid argon. Neutrons moderated and captured in the Gd-PMMA (violet and green), produce γ rays that induce scintillation in the surrounding liquid argon, therefore they are tagged.

background below about 0.1 events over a 200 t·yr exposure, after all the software analysis cuts have been applied.

The Gd-PMMA both reduces and helps tag the neutron background. The high density of hydrogen in PMMA slows the neutrons to thermal velocities and the Gd captures the thermal neutrons resulting in a gamma cascade [6, 7], which is measured in a neutron veto detector surrounding the central TPC and/or in the TPC itself. Events from neutron capture have a different energy scale and hit pattern than single-scatter events from dark-matter interactions. As Fig. 1 shows, eight 15 cm thick panels of Gd-PMMA, each 3.5 m high and 1.6 m wide, form the lateral walls of the TPC volume. Additional blocks (0.4 m by 0.4 m by 0.15 m each) of Gd-PMMA are mounted above the top and below the bottom of the TPC. None of these parts have a structural function: the walls must support their own weight, while the blocks at the top and bottom are supported and held in place by steel structures. For this reason there are no stringent requirements on the mechanical properties of the

Gd-PMMA. The thickness of the Gd-PMMA parts, the gadolinium concentration and its uniformity are the three key requirements set to achieve, given the design of DarkSide-20k, a neutron tagging inefficiency $\sim 10^{-6}$. This number is obtained through a detailed Monte Carlo simulation based on the Geant4 package [8], including the full detector geometry and material composition, with energy thresholds of 200 keV and 50 keV in the Veto and TPC respectively. The result is that the minimum necessary thickness is 15 cm, which comes from a trade-off between the need to moderate and capture the neutron and the need of detecting the capture γ-rays in the surrounding liquid argon. Given this requirement, the raw slabs before processing need to be about 17 cm, as reported in Tab. 1. This is an important requirement for developing the production procedure of Gd-PMMA. Moreover, requiring that neutron capture on gadolinium dominates over neutron capture on hydrogen we found that the optimal concentration of gadolinium is between 0.5% and 1% in weight. Details on concentration and uniformity of gadolinium are given in Sec. 2.2. As described in detail in Sec. 4, the final thickness of a sample is critical for our gadolinium mixing procedure and the subsequent polymerization steps, as the solidification time, and consequently, any non-uniformity in the distribution of the gadolinium depends on the thickness of the final object. Approximately 20 t of material are needed, before all the machining, to build the detector, thus the procedure to produce the Gd-PMMA must be scalable for industrial production.

2.2 Gadolinium concentration and uniformity

The guideline for establishing the concentration is to load the PMMA with an amount of gadolinium such that the capture of neutrons by gadolinium dominates over the same process on hydrogen, thus maximizing the detection probability of the neutrons. Considering the weighted average of all the seven Gd isotopes, the thermal neutron capture on gadolinium σ_{Gd} is $\sim 4.9 \times 10^4$ barns [9], while the thermal capture cross-section on hydrogen, σ_H, is $\sim 3.3 \times 10^{-1}$ barns [10]. (The thermal neutron capture cross-sections on carbon and oxygen are orders of magnitude lower than on hydrogen, thus their contribution to thermal neutron capture is negligible.)

Given these cross-sections, for the probability of a thermal neutron to capture on Gd to be, as a reference, ~ 100 times greater than on H, the Gd concentration in mass needed is $\sim 1\%$ with respect to the PMMA mass. A concentration between 0.5% and 1% still ensures that the capture on gadolinium is dominant, and this range of concentration allows a level of non-uniformity in the Gd distribution over a volume of 1 cm^3. Having a nominal concentration of 1% with a 50% non-uniformity means that in each 1 cm^3 there is at least 0.5% of Gd, so in every point of the material the capture on gadolinium is dominant. For this reason we set a uniformity requirement of 50%. This is a critical aspect when considering the thickness of the samples, because the concentration in the vertical direction can be strongly affected by sedimentation during the solidification. We note the use of nanograins of 80-100 nm in diameter guarantees a substantially continuous distribution when compared with the thermalization length of the neutrons.

The above-mentioned Monte Carlo simulations confirm that a gadolinium concentration between 0.5% and 1% delivers comparable neutron tagging performance given the dominance of σ_{Gd} over σ_H.

2.3 Radiopurity requirements

Requirements about radiopurity are particularly challenging and they are driven by the requirement that the concentration of U and Th in the Gd-PMMA is such that the neutron background contribution of the Gd-PMMA material itself due to (α, n) reactions is subdominant to the total background budget. The γ decays of radioactive contaminants may also generate signals in the same energy range as those produced by WIMPs. However, they are identified and rejected with high efficiency thanks to the different distributions in time and space of the argon scintillation light generated by an energy deposit due to a γ-ray or to a nuclear recoil (that is the hypothetical WIMP interaction) and to the corresponding features of the ratio between scintillation and ionization signals for the two categories of events [11]. The powerful pulse shape discrimination of argon-based detectors makes the γ decays not a significant source of background in the dark matter search. Still, the concentration of γ contaminants must be kept under control to limit the rate of accidental coincidences in the detector that would spoil its performance by introducing a dead time for the WIMP search. An example is the accidental coincidence between a γ-ray induced signal in the neutron veto buffer due to the decay of a contaminant in the detector material (including the Gd-PMMA) and a WIMP-like event in the TPC volume.

The detailed quantitative requirements about the radiopurity depend on the specific design of DarkSide-20k and on a detailed background model, the description of which is beyond the scope of this paper. The output of the backgroud model however provides limits on the activities of the material components, which are reported in Tab.1. The effort performed in screening all the components making the new hybrid material is of general interest in the search for rare events.

2.4 Summary of the requirements

PMMA has been selected as the base material because it is rich in hydrogen and also because it can be produced with an excellent degree of radiopurity through a casting process, polymerizing its liquid monomer (methyl methacrylate, MMA). Since there are no stable commercially available gadolinium compounds that are soluble in liquid MMA, except for some particular very expensive complex compounds like Gadolinium acetylacetonate, we decided to make a dispersion of gadolinium in the liquid monomer followed by the polymerization. We chose to use gadolinium oxide which is a stable and cheap compound, in the form of nanoparticles, to maximize the uniformity of the Gd distribution in the polymer. The characterizations of the samples will mainly focus on verifying the fulfillment of all the mentioned requirements, that are summarized in Tab. 1. From the point of view of the quality of the polymer and its mechanical properties, there are no stringent requirements, as the sheets of the neutron veto will not be subjected to particular mechanical stress, however, some key quantities were measured to verify that Gd-PMMA has similar properties to pure PMMA, as will be shown in Sec. 5.

3 Radiopurity

3.1 Radiopurity of the ingredients

The first step to produce the Gd-loaded hybrid material with the necessary radiopurity is the selection of radiopure components. For this reason, the components of the hybrid material were subjected

Parameter	Value
Gd concentration (weight)	$0.5\% < Gd < 1\%$
Gd homogeneity	$\simeq 50\%$
Transparency of the hybrid Gd-PMMA material	not necessary
Machinable	yes
Stable at 87 K	yes
Thickness [a]	~ 17 cm
Maximum size [a]	sheets of ~ 4 m $\times$ 2 m
^{238}U, ^{235}U, ^{232}Th activity of Gd_2O_3	< 20 mBq/kg
γ contaminants activity of Gd_2O_3	< 2 mBq/kg
Amount needed [a]	about 20 t

Table 1: Target specifications driving the development of the Gd-PMMA. The ^{238}U, ^{235}U, ^{232}Th acceptable concentrations depend on multiple parameters since the background is a combination of values in different parts of the chains with their corresponding yields.

---

[a] Before the machining of the final pieces.

to radiopurity screening using the Inductively Coupled Plasma Mass Spectrometry (ICP-MS) technique or High-Purity Germanium detectors (HPGe). The ICP-MS determines the concentration of an isotope in a sample by measuring mass/charge ratio [12], while an HPGe detector consists of a semiconductor diode that detects traces of unstable isotopes thanks to γ-ray spectroscopy. Most of the assays done with HPGe detectors were carried out in a dedicated facility at the Canfranc Underground Laboratory (LSC), in a radon abated environment [13], while ICP-MS measurements were done at LNGS [14].

The two main ingredients of the Gd-PMMA are MMA (the monomer from which the PMMA is produced), and Gd_2O_3. After a thorough search for suppliers, we have found that commercial gadolinium oxide Gd_2O_3, delivered by the Shin-Etsu Chemical Co. Ltd. Company (Japan) has a suitable level of radioactive contaminants. We selected Gd_2O_3 in the form of nanoparticles with a diameter between 20 and 80 nm, with 3N purity, produced from lots GD-0BB-035 and GD-0BB-038. As reported in Tab. 2, we screened with an HPGe detector three different samples and they show very low contamination levels. In particular the third sample, produced from lot GD-0BB-038, has ^{238}U, ^{235}U ^{232}Th and ^{40}K contamination levels compatible with the background requirements reported in Tab.1.

Concerning MMA, data reported by other experiments show that MMA can both be delivered with excellent levels of radiopurity and contamination during the polymerization phase is avoidable [15, 16], for these two reasons we did not screen the monomer used for the laboratory phase. In the context of the industrial tests described in Sec. 6, an ICP-MS screening was performed on the MMA provided by the selected industrial partner (Clax s.r.l., see Sec. 6 for details). Measurement showed concentrations of thorium and uranium well below the mBq/kg, as reported in Tab. 3. This is a preliminary result that indicates that MMA can generally be a sufficiently radiopure component, a detailed screening should then be carried out once the industrial partner for the final production

Isotope	Gd$_2$O$_3$ Shin-Etsu #1 [mBq/kg]	Gd$_2$O$_3$ Shin-Etsu #2 [mBq/kg]	Gd$_2$O$_3$ Shin-Etsu #3 [mBq/kg]
^{238}U-^{234m}Pa	<1.2·10^3	<637	<99
^{238}U-^{226}Ra^a	13.6±3.0	6.6±1.8	2.68±0.47
^{232}Th-^{228}Ac	<30	<24	<6
^{232}Th-^{228}Th^a	<27	<19	2.31±0.68
^{235}U-^{235}U	<51	<25	<1.5
^{235}U-^{227}Ac^a	<82	<57	<6.5
^{40}K	<37	<24	<13
^{60}Co	<2.5	<1.3	<0.62
^{137}Cs	<4.0	<2.2	<0.70
^{138}La	<3.2	<2.0	<0.71
^{176}Lu	12.9±2.6	12.1±2.1	2.3±0.35

Table 2: Assay results of three Gd$_2$O$_3$ samples from the Shin-Etsu company, performed by the DarkSide Collaboration with a HPGe detector.

^{a} To be compared with the values in Tab.1.

Sample	^{232}Th [mBq/kg]	^{238}U [mBq/kg]
Clax MMA	<0.041	<0.12

Table 3: ICP-MS measurement of the MMA from Clax s.r.l. company used for the industrial tests.

Sample	^{232}Th [mBq/kg] (ICP-MS)	^{238}U [mBq/kg] (ICP-MS)	^{40}K [mBq/kg] (HPGe)
Igepal CO-520	<0.041	<0.12	(31.9±3.2)·10^3

Table 4: Surfactant screening results both from ICP-MS and HPGe. For the full results obtained with HPGe see Tab. 5

has been identified.

In addition to MMA and gadolinium oxide, the hybrid material contains a non-ionic surfactant, Polyoxyethylene (5) nonylphenylether, better known with the commercial name of Igepal CO-520®. This is used to minimize the formation of nanoparticle aggregates, increasing the uniformity of the oxide distribution, as detailed in Sec. 4.1. Compounds such as Igepal CO-520® (nonylphenol ethoxylates) are often produced by the reaction of nonylphenol with ethylene oxide, with the addition of potassium hydroxide as catalyst [17]. The screening carried out with HPGe detector shows, as reported in Tab. 4, that the amount of residual ^{40}K present in the compound is indeed too high for the requirements of the experiment. It was then necessary to develop a procedure, described in Sec. 3.2, to reduce it before its usage.

Finally, during the production of Gd-PMMA, we used two additives necessary to initiate the polymerization, as we will further specify in Sec. 4, but since their concentration is of the order

of ppm and a fraction of their mass is then released in the form of gas during the polymerization reaction, we considered acceptable not to do the screening.

3.2 Potassium reduction in the surfactant

To reduce the [40]K content, the strategy adopted was to perform a purification to remove potassium using an ion exchange resin, a well-known technique [18, 19].

In particular, we adopted the so-called "batch method", often used for non-ionic surfactants, especially with high viscosity, as in the case of the Igepal CO-520®. We used AmberChrom® 50WX4 from Merck Millipore, in the hydrogen form with a 100 mesh (CAS: 69011-20-7). It is a strong cationic resin that removes K^+ and substitutes it with H^+ [20].

The purification strategy is conducted as follows:

1. The resin is washed with ethanol three times until the solvent remains colorless after being in contact with the resin [20].

2. The resin is reactivated with 3M hydrochloric acid.

3. The resin is washed with deionized water and partially dried under a fume hood.

4. The resin, still wet, is immersed in the Igepal CO-520®. The mixture is left under magnetic stirring.

5. The grains of the resin are separated from the purified surfactant with a centrifugation process.

Both the quantity of resin and the stirring time have been optimized during the tests, informed by several measurements of the potassium content. In particular, the purified Igepal CO-520® was screened with Inductively Coupled Plasma Atomic Emission Spectrometry (ICP-AES). Some of the prepared solutions were also screened via ICP-MS, to crosscheck the measurements. The best purification procedure consists of using $10\%_w$ of resin, with respect to surfactant mass, and keeping them under magnetic stirring for one week. One of the final samples, purified with this procedure, underwent HPGe screening, to evaluate the concentration of all the contaminant isotopes. Results are reported in Tab. 5 and it can be seen that the [40]K activity was reduced by about a factor of 250.

In parallel to the tests of the procedure with the ion exchange resin, we decided to reduce the amount of surfactant used in the polymerization process. In the laboratory tests, we reduced up to a factor 100 the Igepal CO-520® amount, going from $1\%_w$ with respect to the MMA mass, as used in our standard procedure, to $0.01\%_w$. In the industrial tests, we opted for a surfactant concentration of $0.1\%_w$, since the polymerization is more delicate. This reduction is sufficient to achieve contamination values acceptable for the experiment. Moreover, by combining the reduction in mass with the purification a considerable safety margin on the amount of potassium can be achieved.

4 Laboratory production

As mentioned in Sec. 1, Gd_2O_3 is not soluble in liquid MMA, so it is necessary to make a dispersion to mix them together. The use of commercial Gd_2O_3 in the form of nanoparticles with a diameter

Isotope	Raw Igepal activity [mBq/kg]	Purified Igepal activity [mBq/kg]
^{235}U	<51	<9.4
^{238}U-^{234m}Pa	<4.8·10^3	<1.5·10^3
^{238}U-^{226}Ra	<55	<19
^{232}Th-^{228}Ac	<105	<43
^{232}Th-^{228}Th	<43	<12
^{40}K	(31.9±3.2)·10^3	129±24
^{137}Cs	<28	<4.4
^{60}Co	<23	<3.3

Table 5: Results of the assay campaign conducted on both the raw and the purified surfactant. The screening was performed with a HPGe detector.

between 20 and 80 nm, maximizes the uniformity of the Gd distribution in MMA. As reported in Tab. 1, a gadolinium concentration in mass between $0.5\%_w$ and $1\%_w$ is necessary for the final material. The laboratory work was started aiming at obtaining a stable colloidal dispersion of gadolinium oxide in liquid MMA with a very small concentration ($0.001\%_w$ of Gd_2O_3). Then the concentration was progressively increased up to a maximum of $2\%_w$ of gadolinium, corresponding to $2.3\%_w$ of Gd_2O_3, considering the molecular mass. The maximum concentration value tested was chosen to have a large safety margin, since it is twice the maximum required value.

To get a uniform distribution of Gd_2O_3 with a concentration up to $2.3\%_w$, it is necessary to treat the nanoparticles in advance, to minimize the formation of aggregates and prevent their sedimentation. It is indeed well known that nanoparticles tend to cluster and, consequently, deposit on the bottom of the mold during the polymerization process, spoiling the uniformity of the final material [21]. The basic idea is to treat the nanoparticle's surface to undergo a functionalization process. Functionalization refers to the surface modification of nanoparticles, which includes the bonding of chemicals or biomolecules onto the surface aimed at creating repulsive electrostatic forces and steric hindrance factors (that is the prevention or retardation of interaction as a result of a spatial structure of a molecule) [22, 23]. This is the first step of the developed procedure and it is performed by treating the nanoparticles with a commercial non-ionic surfactant in a non-aqueous solvent. This process introduces a repulsive force between the particles that stabilizes the dispersion. The second step consists in the polymerization phase, which has been optimized to produce thick (up to 22 cm) samples. In particular, the polymerization time depends on the sample thickness, since as the thickness increases, also the solidification time does, consequently a Gd_2O_3 deposit is more likely to form. To overcome this effect a procedure was required to fine-tune the polymerization temperature, the quantities of chemical initiators used, and the pre-polymerization phase.

4.1 Surface treatment of the nanoparticles

As anticipated in Sec. 3.1, to facilitate the dispersion of the Gd nanoparticles we chose to perform the functionalization with Polyoxyethylene (5) nonylphenylether, branched (($C_2H_4O)_n \cdot C_{15}H_{24}O$),

whose commercial name is Igepal CO-520®, by Sigma Aldrich. It is a non-ionic commercial surfactant that appears as a transparent and viscous liquid. Gadolinium oxide and surfactant are added, in a 1:1 mass ratio (so both at $1\%_w$ with respect to MMA), to a non-polar solvent, which is taken in a ratio of about 1:4 to the MMA, by volume. 2-butanone (Sigma Aldrich, $\geq 99.0\%$) was chosen as the non-polar solvent due to its boiling temperature (79.6℃) which allows it to easily evaporate in the first minutes of the pre-polymerization phase. Moreover, the boiling temperature is high enough to not create bubbles during the polymerization phase, if traces of 2-butanone remain in the sample after the pre-polymerization. The mixture is then sonicated, in order to break up any agglomerate of nanoparticles and to favor their surface covering with the surfactant. This procedure is carried out for 15 minutes in continuous mode, using a Sonic Ruptor 400 Ultrasonic Homogenizer, by Omni.

As anticipated in Sec. 3.2, several tests have been performed to reduce the amount of surfactant, in order to minimize the radioactive contamination. The described steps have been performed both with $0.1\%_w$ and $0.01\%_w$ of Igepal CO-520® with respect to the monomer. These samples were characterized to evaluate the uniformity of the Gd distribution even in the presence of a lower quantity of surfactant (see Tab. 10 in appendix A). Based on the results of the characterization, we can state that the procedure is successful also using $0.01\%_w$ of surfactant.

4.2 Polymerization

Since methylmethacrylate is a non-viscous liquid, during the polymerization phase clusters of nanoparticles form, and consequently an oxide deposit is created at the bottom of the mold. This happens even with treated nanoparticles because of the long polymerization time: the dispersion of treated gadolinium oxide remains stable for roughly one hour (see Sec. 5), while the full polymerization takes up to 24 hours.

Therefore, to minimize the formation of a Gd_2O_3 deposit, we perform the polymerization in two steps [23]: first, we start a pre-polymerization phase, during which the MMA viscosity increases due to the formation of a pre-polymer (or oligomer), and then the actual polymerization occurs, leading to the final solid polymer.

As a preliminary operation, the MMA is passed through a separation column containing aluminum oxide (Al_2O_3), to remove hydroquinone monomethyl ether (MeHQ), which is used as the stabilizer and polymerization inhibitor. Once the MMA is filtered, the sonicated dispersion of gadolinium oxide (prepared as described in Sec. 4.1) is added. The mixture is then heated on a plate and frequently stirred manually. During this phase, the 2-butanone solvent starts to evaporate. When the temperature reaches 80℃, 100 ppm of primary polymerization initiator, with respect to the MMA mass, is added. AIBN (2,2-Azobis (2-methylpropionitrile $(CH_3)_2C(CN)N{=}NC(CH_3)_2CN)$) was used as initiator. When the temperature is between 94℃ and 100℃, a very vigorous boiling begins due both to the reaching of the boiling point of the monomer, and to the splitting of the AIBN, which produces gaseous nitrogen. At this point the viscosity of the mixture rapidly increases, because the initiator causes the start of the radical polymerization reaction. The heating is stopped after 9 minutes of boiling when a homogeneous whitish viscous mixture is obtained. At this point, the 2-butanone solvent is fully evaporated.

The second phase of the process starts with removing the beaker from the heating plate. Then, 600 ppm (with respect to the MMA mass) of secondary initiator are added, namely Lauroyl peroxide

Figure 2: Sample 22 cm high, obtained starting from 600 g of MMA, loaded with $2\%_w$ of Gd (equal to $2.3\%_w$ Gd_2O_3).

98% ($[CH_3(CH_2)_{10}CO]_2O_2$), whose commercial name from Sigma Aldrich is Luperox. The whole compound is mixed manually, to dissolve the Luperox and finally, it is transferred in a glass mold and placed in the oven at 55℃, for 24 hours. Consequently, the sample is completely solid.

4.3 Samples produced at the laboratory scale

Numerous samples were made, varying some of the parameters described above. The gadolinium oxide and the surfactant concentrations were progressively modified throughout the optimization of the procedure, reaching $2.3\%_w$ for the Gd_2O_3 and $0.01\%_w$ for the Igepal CO-520®.

Another key aspect was the optimization of the procedure to maximize the thickness of the samples, to reach the 17 cm required. It was possible to produce samples with a thickness greater than 20 cm, as the one shown in Fig. 2 that, in particular, was produced with a $2.3\%_w$ concentration of Gd_2O_3 and $2.3\%_w$ of Igepal CO- 520®. To obtain a sample with these characteristics, the mass of MMA was progressively increased in the various productions, also varying the other parameters of the procedure.

5 Characterization

During the laboratory test phase, different aspects of the produced samples have been characterized. The procedures and the techniques described in this section were then applied to verify the quality

of the industrial-scale samples (Sec. 6).

In particular, we report on the following aspects:

1. Characterization of the surface treatment (Sec. 5.1);

2. State of the polymeric matrix (Sec. 5.2);

3. Homogeneity of the Gd_2O_3 distribution (Sec. 5.3);

4. Mechanical tests (Sec. 5.4).

5.1 Characterization of the surface treatment

The efficiency of the nanoparticles surface treatment procedure has been evaluated through two different types of measurements: the Fourier-Transform Infrared Spectroscopy (FTIR) [24] and Dynamic Light Scattering (DLS) [25]. The FTIR technique allows the identification of chemical substances or functional groups present in the sample. Our measurements have been performed using the Alpha II compact spectrometer by Bruker, in a wavenumber range from 4000 cm^{-1} to 500 cm^{-1}. The functionalization is singled out by comparing the IR absorption spectra of the treated nanoparticles - after the functionalization procedure - with that of the raw Gd_2O_3 and raw surfactant. The treated samples were always in the form of dried powder, while the raw surfactant was in liquid form. Fig. 3 shows the infrared spectra of the two raw ingredients superimposed on the spectrum of a functionalized sample. The nanoparticles covering is evidenced by the presence, in
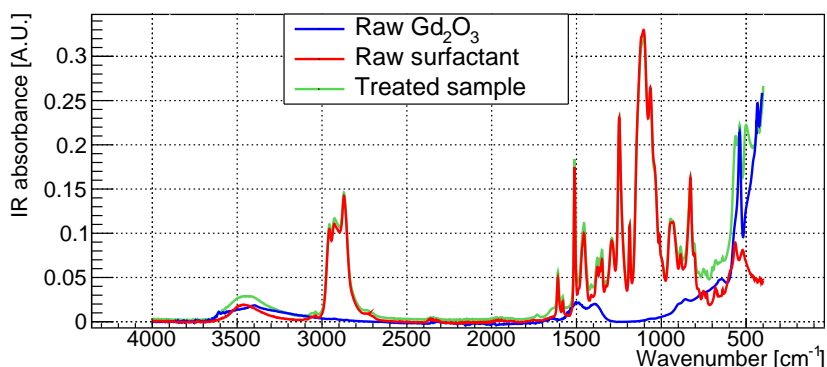

Figure 3: IR spectra of the pure gadolinium oxide (blue), the pure surfactant (Igepal CO-520, orange), and the treated sample (green).

the spectrum of the treated sample, of the characteristic peaks of the surfactant (the region between 700 and 1500 cm^{-1} and between 2700 and 3000 cm^{-1}) in addition to those of the gadolinium oxide (as can be seen in the region around 500 cm^{-1}). This result can be considered as a first qualitative indication of the presence of the surfactant on the nanoparticles.

Additional information has been obtained with the DLS technique, used to analyze the colloidal stability of the treated Gd nanoparticles in liquid. The basic idea is to perform various DLS measurements as a function of time, to investigate the hydrodynamic size of particles (or clusters of nanoparticles) that have remained in suspension after a certain time. The variation of the particle
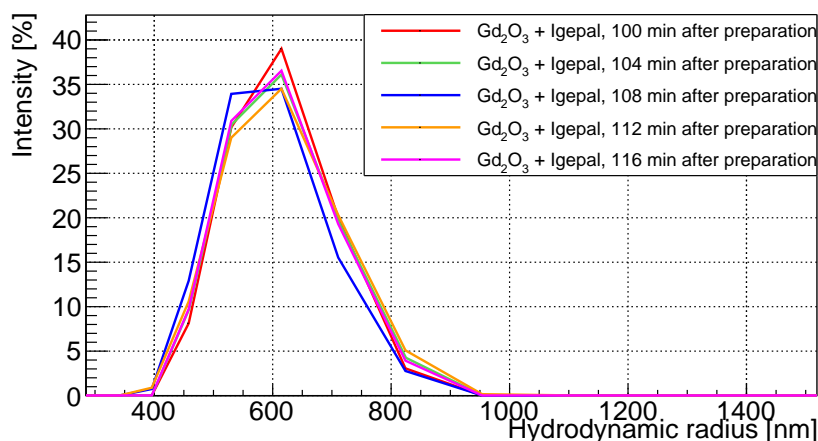
Figure 4: DLS measurements performed on a sample carrying an equal concentration of surfactant and Gd_2O_3 nanoparticles, diluted to a concentration of 0.4 mg/ml. The different curves were acquired starting 100 minutes after the preparation of the sample, at 4-minute intervals. The plot shows that in the 20-minute duration of the measurement, the population of nanoparticles with a hydrodynamic radius peaked at 600 nm is well reproducible, and therefore the suspension is stable.

hydrodynamic size distribution over time can give an indication of their sedimentation. The DLS technique is based on the study of the Brownian motion of dispersed particles, from which it is possible to determine their hydrodynamic diameter by measuring their speed thanks to the Stokes-Einstein equation. The instrument used is the Zetasizer nano ZS90 by Malvern Panalytical. The light source used is a 10 mW 632.8 nm He-Ne laser, with an optical detector at 90°.

After the sample was prepared as described in Sec. 4.1, the suspension - just at the end of sonication - is diluted with pure 2-butanone, reaching a concentration of about 0.4 mg/ml. However, in 2-butanone, and in general in low-viscosity solvents, it was not possible to obtain a fully stable dispersion on which to carry out a quantitative analysis. Although the dispersion is not entirely stable, the role of the surfactant is still crucial and to highlight the effect caused by its presence, it was decided to perform a DLS measurement by comparing a treated sample with an untreated one, i.e. free of surfactant. Moreover, in order not to alter the dispersion, the sample was left inside the instrument for the entire duration of the measurement. The two analyzed dispersions were obtained applying the exact same procedure (see Sec. 4.1), but avoiding the addition of the Igepal CO-520® in one of the two.

The results obtained with the bare Gd_2O_3 nanoparticles were unsatisfactory, since the data did not even meet the basic quality requirements of the software of the instrument. This means that the suspension is not stable even on time scales of 15-20 minutes, which is the time required to complete the measurement, and very fast sedimentation of the nanoparticles occurs. On the other hand, the functionalized sample showed results that satisfied the data-quality controls, i.e. the stability of the suspension is compatible with the characteristic time scales of the measurement. So, it was possible to perform several measurements at different times after the end of the sonication. Analyzing the particle hydrodynamic size distribution over time, there is evidence of sedimentation, so the suspension with the surfactant is not completely stable, as mentioned previously. However, 100

minutes after the end of the sonication, there is still a clear population of nanoparticles dispersed, with a hydrodynamic radius of around 600 nm, as reported in Fig. 4. In conclusion, the surface treatment does not allow the production of a fully stable suspension but reduces the clusterization and, therefore, the sedimentation. The results obtained with the functionalized nanoparticles are greatly improved with respect to the ones of the unfunctionalized Gd_2O_3.

The functionalization procedure, combined with the developed polymerization procedure, allows to obtain Gd-PMMA samples with a good nanoparticles distribution (as it is evidenced from the characterization in Sec. 5.3).

5.2 State of the polymeric matrix

The effect of the presence of the nanoparticles in the polymeric matrix has been evaluated by looking for possible differences in the glass transition temperature (T_g), which is one of the most important parameters to evaluate the thermomechanical properties of a polymer [26]. The T_g value is obtained through Differential Scanning Calorimetry (DSC) using a DSC1 Star^e System by Mettler Toledo. At the glass transition temperature, there is a variation of the specific heat, detectable from the DSC curve. In particular, we have adopted the most widely used definition, according to which the midpoint T_g is defined as the point at which the first derivative of the DSC curve is maximum. Three thermal ramps were carried out: the first, in heating, from room temperature to 250℃, the second, for cooling, from 250℃ down to -50℃ and the last, a second heating phase, from -50℃ to 250℃. The glass transition temperature found for all samples, prepared with an identical procedure, is between 116℃ and 119℃. Considering the non-negligible uncertainty associated with the DSC technique, the values are considered fully compatible [27]. This means that the developed procedure leads to a hybrid material with reproducible properties from the point of view of the polymer matrix. Moreover, the presence of Gd_2O_3 does not cause significant variations of the T_g with respect to the pure PMMA reference values [28, 29].

5.3 Homogeneity of the Gd_2O_3 distribution

To characterize the homogeneity of the Gd_2O_3 distribution along the whole height we have analyzed portions of the same sample, taken at different heights starting from the bottom of the mold, as illustrated in Fig. 5. The measured samples have been divided into several sections, depending on the height of the sample itself (usually the highest part, the central part, and the lowest part). Subsequently, fragments of each section have been weighed with a precision balance, and placed in an alumina crucible, which in turn was placed in a tubular oven open at the ends, to facilitate the escape of gases. The sample was calcinated, i.e. heated up to 600℃, to remove all the organic substances, through thermal decomposition [30]. In particular, the standard thermal cycle consisted of initial heating from room temperature to 300℃, followed by a second heating ramp up to 430℃, and, finally, the sample was brought to 600℃. Each of these temperatures was kept constant for 20 minutes. Subsequently, the sample was slowly cooled to 250℃ and, finally, to room temperature. At the end of cooling in the crucible only inorganic residues are present. In our case the residue consists only of the gadolinium oxide initially present in the portion of the sample analyzed. By weighing the residue and comparing the result with the initial mass, a measurement of the Gd_2O_3
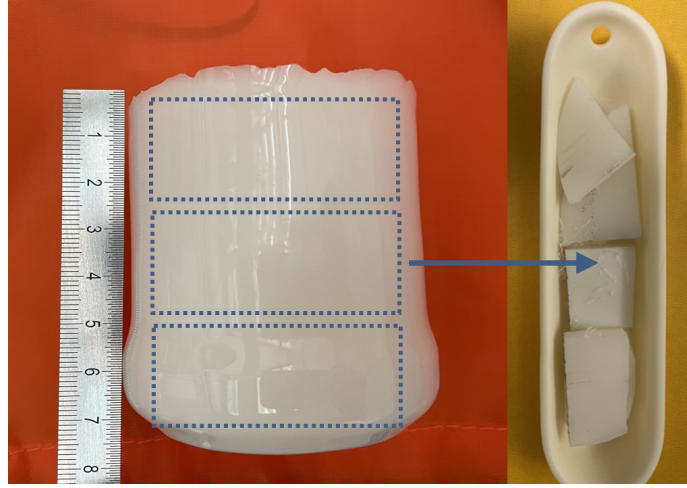
Figure 5: Scheme of samples sectioning for the calcination tests.

concentration ($C_{Gd_2O_3}$) by weight is obtained, following:

$$C_{Gd_2O_3} = \frac{100 \cdot m_{Gd_2O_3}}{m_{Gd\text{-PMMA}}} \, ,$$

where $m_{Gd_2O_3}$ is the mass of the Gd_2O_3 residue after the thermal cycle, and $m_{Gd\text{-PMMA}}$ is the mass of the starting Gd-PMMA sample portion subjected to this analysis. By analyzing the different sections, the uniformity of the distribution of Gd_2O_3 along the vertical direction of the sample is obtained. The most significant results are reported in Fig. 6. In this figure, the y-axis reports a concentration difference ΔC, which expresses the difference between the measured Gd_2O_3 concentration and the nominal one.

Samples 1, 2, and 3 carry a concentration equal to $1\%_w$ of Gd_2O_3 and an equal concentration of surfactant, they are respectively 3 cm, 7 cm, and 11 cm thick. Sample 4 is 8.5 cm thick, and has a Gd_2O_3 and Igepal concentration of $2.3\%_w$ and $2\%_w$, respectively. Finally, Sample 5 is 20 cm high and carries a concentration of $1\%_w$ Gd_2O_3 and $0.1\%_w$ Igepal, it was obtained following the final procedure. Thanks to the procedure used and the thermal cycle inside the muffle furnace, we do not expect any external contamination that could have increased the inorganic residue. However to study any systematic effects and verify the presence of inorganic residues other than gadolinium oxide, we also performed the same thermal treatment on a pure PMMA sample. We did not find any residual component, the difference between the initial and final masses is zero, within the error margin of the balance.

We can therefore conclude that the procedure described in the previous sections leads to homogeneous samples. With the exception of the lower section of sample 4, where there is a greater deposit, all the samples shown in Fig. 6 have an uniformity within 50%, as required. It is useful to observe that the concentration variations are always greater than zero, this is due to the evaporation of a few grams of MMA during the polymerization phases.

In Tab. 10 in appendix A, calcination results obtained on a wider range of laboratory samples are reported. Those tests have been done in order to investigate the reproducibility of the homogeneity results, both increasing the height of the samples and the Gd_2O_3 concentration.
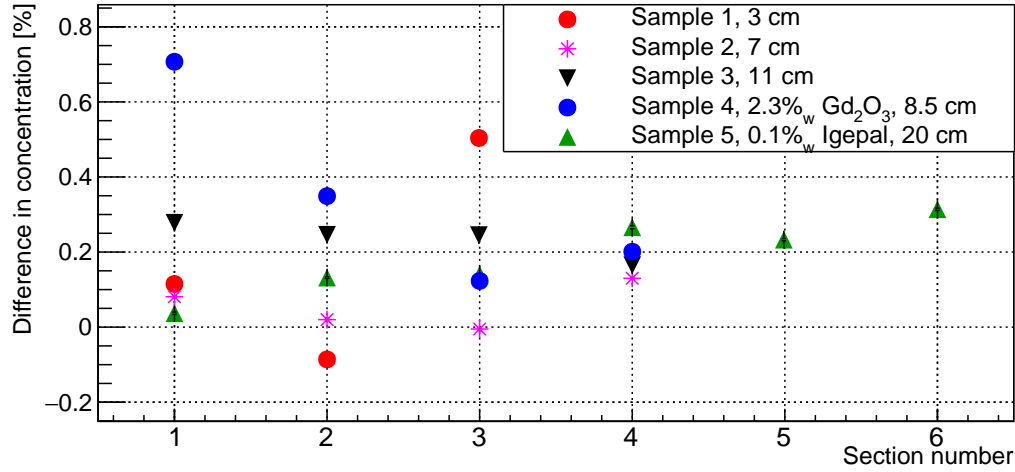
Figure 6: Results of the most representative calcination tests. On the y-axis, ΔC is the difference between the measured and the nominal mass concentration (expressed in $[\%_w]$) values. Referring to Tab.10, the plot shows the difference between the fourth and the third columns for samples: 19-05-2, 26-05-2, 29-09-1, 05-10-1 and 09-12-1, here called 1,2,3,4 and 5 respectively. In all displayed plots, the y errors are covered by the markers.

5.4 Mechanical tests

As anticipated in Sec. 2 we used the characteristic values of pure PMMA as a benchmark to which we compared some mechanical properties of Gd-PMMA. It was decided to measure, among all the mechanical properties, Young's modulus and the tensile strength because they are often used as key basic properties and also because they can be measured through simple and quick tensile tests.

Since for the DarkSide-20k experiment, operation at temperatures around 87 K is required, it was also necessary to cool the samples to cryogenic temperature and check their integrity. In addition, after a visual inspection, it was important to repeat the measurement of the mechanical properties to estimate any possible effects due to the cooling cycles.

Before performing any cool down or mechanical test, we annealed the samples to reduce all the residual stresses possibly accumulated during the polymerization and the mechanical machining. The thermal cycle was carried out in an oven, which can be either static or ventilated, and consisted of three phases: the heating ramp, the isothermal phase, and the cooling ramp. During the first phase, the temperature is increased, starting from room temperature, by 20℃ every hour, until reaching 85℃. This temperature - close to T_g, but still more than 20℃ below - is then maintained for 20 hours. Finally, a very slow cooling phase starts: temperature is decreased by 5℃ every hour, down to room temperature. This procedure does not alter the properties of the polymer: this has been proven by comparing the glass transition temperature of annealed and not annealed portions of the same samples (see the DSC curves reported in Fig. 7). Note that the T_g of this sample is different from the one reported in Sec. 5.2, but still in the range of pure PMMA. The samples, after the annealing process, were cooled down to 77 K by immersing them in liquid nitrogen. Since the Gd-PMMA will be used in liquid argon, i.e. at 87 K, the test in liquid nitrogen is conservative. The
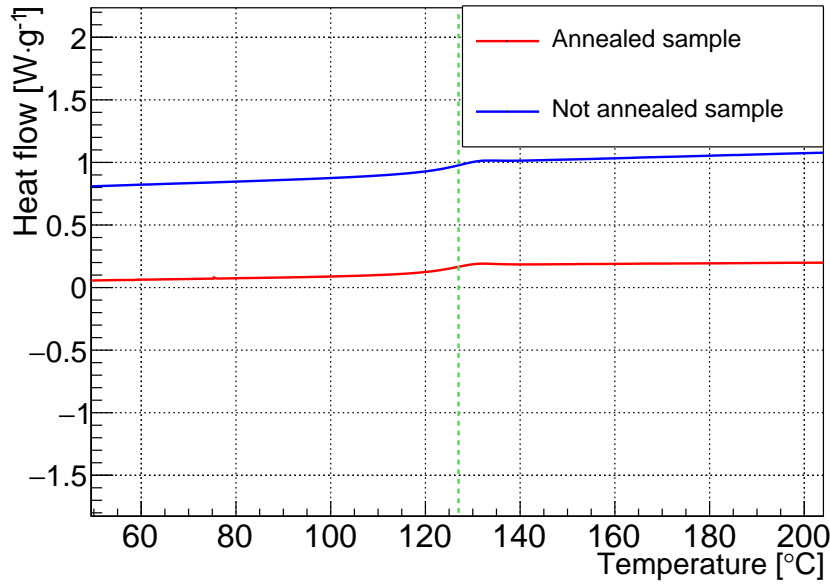
Figure 7: DSC curves of two specimens derived from the same sample, one annealed (blue) and the other not (red). The green dotted line is found in correspondence with the T_g value for both specimens (around 127℃), which has not changed as a result of the thermal cycles.

cooling from room temperature was performed using cold gas nitrogen during the first phase and then gradually submerging the sample with liquid nitrogen. Throughout the process, temperatures in different points of the sample were monitored - using Pt-100 sensors - and cooling was adjusted so that the maximum temperature gradient did not exceed 50℃. Samples of various thicknesses (from 1 mm to 20 cm) have been cooled and have been maintained in LN_2 from a few hours up to 2 weeks. None of the samples showed any sign of damage or degradation when visually inspected after the thermal cycle. In some cases, after the annealing step and a complete thermal cycle, the samples were subjected to a tensile test. One of the results is reported in Fig. 8. The Young's modulus of this sample is 1.3 ± 0.1 GPa, obtained from the fit of the curve in the elastic region, while the ultimate tensile strength is 32.28 ± 0.04 MPa. Young's modulus values of samples subjected to annealing and a full thermal cycle do not show significant variations compared to the values of pure PMMA usually found in the literature, which are between 0.6 GPa and 3.3 GPa [31, 32]. Therefore we can conclude that neither the presence of nanoparticles in the polymeric matrix, nor the treatments undergone significantly modify the mechanical properties compared to pure PMMA.

6 Industrial scale tests

Since the amount of material required for the DarkSide-20k experiment is about 20 t, an important part of the activity consisted in transferring the procedure - validated at the laboratory scale - to an industrial production line. We chose as partner an Italian company, Clax Italia s.r.l. [33]. The transfer of the technology required an optimization of the mixing and polymerization procedures
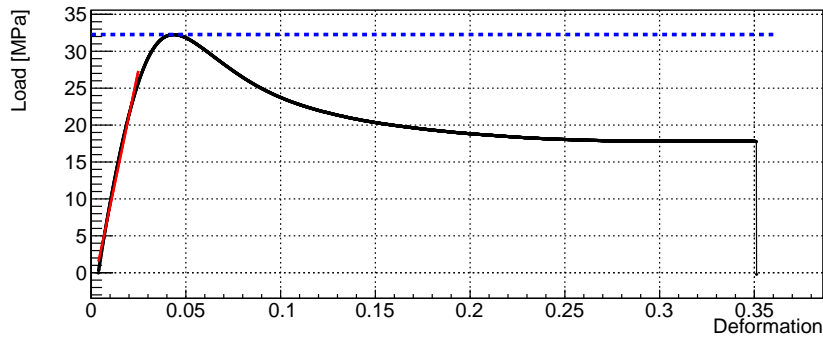
Figure 8: Stress-strain curve of a sample subjected to a cooling cycle in LN_2. The deformation is adimensional, since it is defined as $\Delta L/L$. The red line was used to fit the stress-strain curve in its elastic region for the calculation of the Young modulus, while the blue dotted line underlines to the yield stress value for this sample.

to adapt them to the production of large masses (in the order of tens of kilograms) and to the infrastructures available at the company. The key aspect on which the technology transfer work was concentrated was the viscosity setting to maximize the homogeneity of the gadolinium distribution. The final industrial procedure involves a first mixing phase when the Gd_2O_3 nanoparticles and the Igepal CO-520® are directly incorporated in a small quantity of MMA and subjected to vigorous mechanical stirring. Then this mixture is added to the final amount of MMA and the pre-polymerization stage is performed in a dedicated reactor, which consists of a heated container with a mechanical stirrer. During this phase the viscosity increases: as said, various tests were carried out, varying the duration and heating during this phase, reaching different viscosity values, as shown in Tab. 6. Finally, the high-viscosity syrup is injected into a glass mold which is kept under high pressure during the polymerization in an autoclave. The polymerization time depends on the thickness of the sample: for the 12 cm thick sheets the full thermal cycle in autoclave has lasted 12 days. Several large-scale samples were produced, varying not only the viscosity but also the amount and type of additives. Some of the 12 cm thick sheets produced are shown in Fig. 9 Entering into the details of each procedure is beyond the scope of this work, but a summary of the main parameters is presented in Tab. 6. Note that the use of 2-butanone as a solvent for the preparation of the suspension, which was adopted in the first three industrial samples, was then removed, further simplifying the procedure. Thanks to the use of a dedicated reactor, both the mixture was kept continuously under mechanical stirring, and the viscosity was increased during the pre-polymerization phase, up to 1000 cP, thus making it possible not to use a liquid solvent to ensure the uniformity of the nanoparticles distribution.

6.1 Industrial samples characterizations

The characterization of industrial samples was initially focused on the uniformity of the nanoparticles distribution. Following the procedures developed during the laboratory test phase, the homogeneity was measured by exploiting the calcination technique. The sheets have been cut in six sections at different heights with respect to the bottom of the mold. Small fragments from each section were subjected to the thermal cycle described in Sec. 5.3, then the inorganic residue, corre-

Sample name	Surface [cm²]	Thick. [cm]	Gd₂O₃ [%$_w$]	Igepal [%$_w$]	T [°C]	P [bar]	Solv. [y/n]	Visc. [cP]
Clax 1-1	40×40	4	1	1	Std	1	yes	400
Clax 1-2	40×40	4	1	1	Std	1	yes	400
Clax 1-3	40×40	4	1	1	Std	1	no	400
Clax 2-1	50×50	12	1	0.1	≈50	10	no	1000
Clax 2-2	50×50	12	1	0.1	≈50	10	no	1000
Clax 2-3	50×50	12	1	0.1	≈50	10	no	1000
Clax 2-4	50×50	12	0.80	0.1	≈50	10	no	400
Clax 2-5	50×50	12	0.85	0.1	≈50	10	no	400

Table 6: An overview of the samples produced at Clax Italia s.r.l.. In addition to the variations of the parameters shown in the table, the procedures involved other small modifications from one sample to the other (addition of cross-linking agents, chain transfer agents, etc.). The column "Solv." indicates if the solvent was used or not, the column "Visc." indicates the value of the viscosity in the syrup. "Std" means that the company followed its standard thermal cycle used for pure PMMA, the details were not shared with us.

Figure 9: Picture of four 12 cm thick sheets produced at Clax Italia s.r.l.

sponding to the Gd₂O₃ was precisely weighed. We report in Fig. 10 the results obtained with the 12 cm thick sheets produced. They show that the industrial procedure was successful in producing a sheet with a thickness that is 70% of the one needed for the DarkSide-20k experiment. The results of the uniformity of the gadolinium oxide distribution, give an indication that the same procedure can lead to satisfactory results even with thicker plates. Furthermore, since there is still room to increase the polymerization speed and tune the viscosity of the pre-polymer, we are confident to obtain sheets of 17 cm thickness.

Based on the results of the measurement of the uniformity of Gd₂O₃ and of the visual inspection aimed at identifying any macroscopic defects in the samples, the sheet named "Clax 2-3" was selected as the best candidate. On the latter, further characterizations were then carried out, following what was done for the laboratory scale samples. For what concerns the glass transition
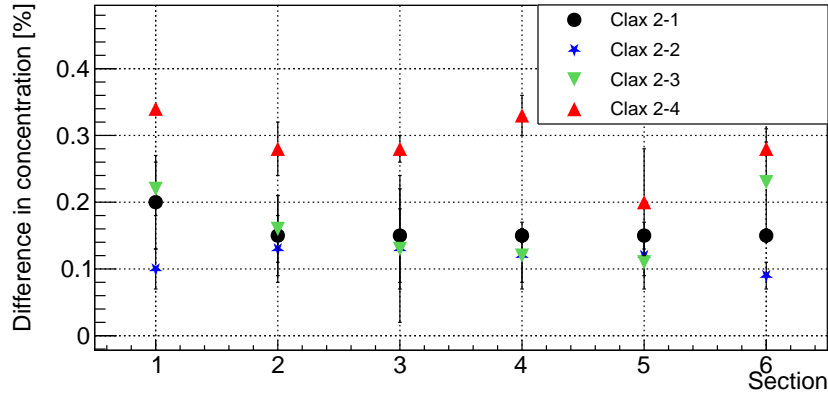
Figure 10: Deviation from the nominal value of the Gd_2O_3 concentration in six sections, taken at different heights. The results for four different sheets are reported.
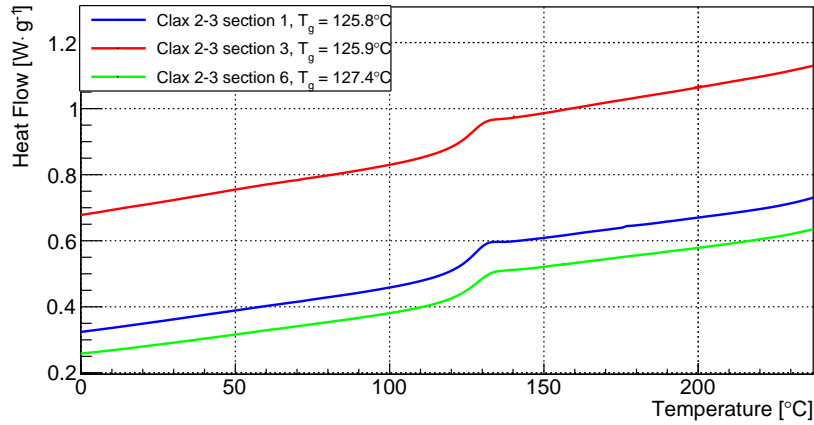

Figure 11: DSC curves different sections of the sample Clax 2-3. The reported T_gs fall within the systematic uncertainty equal to $\pm 2.5°C$ obtained from reproducibility measurements carried out on a single sample of Gd-PMMA. The T_g is thus compatible along the sample's thickness.

temperature, results are reported in Fig. 11 and it can be seen that the value is uniform across the sheet and compatible with the one of pure PMMA. The mechanical properties were investigated with tensile tests and thermomechanical tests, in order to derive the coefficient of thermal contraction. As for the tensile tests, the values of Young's modulus and ultimate tensile strength are reported in Tab. 7. To calculate the thermal contraction coefficient, a test was conducted, which consists in cooling a homogeneous sample of PMMA doped with Gd_2O_3 in LN_2, which is then left to thermalize for a few hours. Then the dimensions of this sample are measured with a caliper, after having quickly extracted it from the cryogenic bath. The dimensions are then compared to those that had been measured at room temperature, prior to cooling. This measurement was made on a parallelepiped taken from the Clax 2-3 industrial sample. For each face of the parallelepiped we measured the width and length, along two axes perpendicular to each other (named "a" and "b") and parallel to the face under examination. Then, the coefficient of linear thermal expansion (CLTE)

Specimen	Young Modulus [GPa]	Ultimate tensile strength [MPa]
Clax 2-3 a	1.4 ± 0.2	44.05 ± 0.05
Clax 2-3 b	1.2 ± 0.2	39.29 ± 0.03

Table 7: Mechanical properties of our best industrial-scale sample. The specimen Clax 2-3 a was subjected to cooling in LN_2, while the other one (Clax 2-3b) was not. Therefore, the exposure of our samples to very high thermal cycles does not influence the mechanical properties.

was calculated according to Eq. 6.1

$$\alpha_L = \frac{1}{L} \cdot \frac{dL}{dT} \tag{6.1}$$

where L is the length of the sample considered and T is the temperature. The results are reported in Tab. 8. After that, the average value of all the measurements was calculated to obtain an estimate of

Face:	Axis:	Length (T_{amb}) [mm]:	Length (T_{LN_2}) [mm]:	α_L [K^{-1}]:
Bottom	a	104.7	103.95	$(3.24 \pm 0.06) \cdot 10^{-5}$
	b	107.53	106.62	$(3.83 \pm 0.06) \cdot 10^{-5}$
Top	a	105.24	103.68	$(6.7 \pm 0.07) \cdot 10^{-5}$
	b	107.58	106.43	$(4.84 \pm 0.07) \cdot 10^{-5}$
1	a	117.86	116.24	$(6.22 \pm 0.07) \cdot 10^{-5}$
2	a	117.88	116.37	$(5.80 \pm 0.07) \cdot 10^{-5}$
3	a	117.81	116.64	$(4.49 \pm 0.06) \cdot 10^{-5}$
4	a	117.87	116.62	$(4.80 \pm 0.06) \cdot 10^{-5}$

Table 8: Thermal contraction measurements on a specimen taken from the industrial sample Clax 2-3.

the contraction coefficient, which is equal to $(4.99 \pm 0.02) \cdot 10^{-5}$ K^{-1}, in line with what is reported in the literature for the pure PMMA [32].

6.2 Industrial samples radiopurity

In addition to the screening of the three main ingredients of Gd-PMMA (MMA, Gd_2O_3 and Igepal CO-520®) reported in Sec. 3.1, we also measured a sample of Gd-PMMA from Clax s.r.l. to evaluate any eventual contamination that may be caused by the industrial production process. The results are reported in Tab. 9. The sample under screening was produced during the second cycle of tests at this company, following the optimized procedure to obtain large mass thick sheets described before.

It is important to underline that the surfactant amount used to obtain this sample is $0.1\%_w$ with respect to the MMA initial mass, but the surfactant had not been purified following the procedure described in Sec. 3.2. As anticipated the surfactant reduction alone already shows good results, but moreover we are reasonably sure that by applying the purification procedure the requirements

Isotope	A [mBq/kg]
^{235}U	< 0.64
^{238}U/^{234m}Pa	< 17
^{238}U/^{226}Ra	< 0.26
^{232}Th/^{228}Ac	0.4 ± 0.2
^{232}Th/^{228}Th	0.4 ± 0.2
^{40}K	14 ± 3
^{137}Cs	< 0.24

Table 9: Screening performed with HPGe detector on Clax gadolinium loaded PMMA. The sample that has been screened is "Clax 2-3", see Tab. 6 for the production details.

reported in Tab.1 could be satisfied. This could be one of the future developments following this work.

In conclusion, considering the activities of the main ingredients and one of the final samples we can state that the production on the industrial line does not cause any significant contamination and is therefore usable for the production of Gd-PMMA for an experiment with stringent radiopurity requirements as DarkSide-20k.

7 Conclusions

The goal of this work, carried on within the context of DarkSide-20k as one of the several R&Ds, was to develop a new plastic hybrid material, made of a polymeric matrix rich in hydrogen and homogeneously loaded with gadolinium in high concentration. The material has to be ultra-pure from the radioactivity point of view and capable to survive at cryogenic temperatures. The strategy adopted was to use gadolinium oxide nanoparticles to create a mechanical dispersion in liquid MMA and then polymerize the mixture.

To minimize the clustering of the nanoparticles and the eventual sedimentation, the gadolinium oxide was functionalized with a commercial non-ionic surfactant, which introduces repulsive forces and steric hindrance. The efficiency of this first step of the procedure has been evaluated by performing FTIR and DLS measurements. The results indicate the presence of the surfactant on the nanoparticles and that the stability of the Gd_2O_3 dispersion is of the order of one hour.

The polymerization procedure, done in two steps, using two different chemical initiators, was optimized to obtain uniform thick samples, with a concentration of Gd up to $2\%_w$.

The hybrid material was tested to verify if the presence of nanoparticles influenced the thermo-mechanical properties of the polymeric matrix. DSC measurements show that the glass transition temperature does not change due to the presence of the treated nanoparticles.

The uniformity of gadolinium oxide distribution was verified for nearly all laboratory-scale samples, using the calcination technique. The results are satisfactory for sample heights up to 20 cm: this proves the feasibility of the process, to obtain 17 cm thick samples compliant with DarkSide-20k requirements. Also, the mechanical characterization of the laboratory scale samples show that the presence of nanoparticles does not spoil the analyzed mechanical properties with respect to the pure

PMMA. The samples have also passed the cryogenic tests.

The developed mixing procedure was successfully transferred to a partner company, Clax s.r.l., where it was optimized to obtain 12 cm thick sheets. These industrial samples have been characterized following the procedures developed during the laboratory phase, and have met all the requirements. In particular, the Gd_2O_3 uniformity, which was the most critical aspect, has been improved with respect to the laboratory samples and it is fully compatible with the requirements. Finally, we were able to reach the required levels of radiopurity, both for the single ingredients and for the final Gd-PMMA. In conclusion, the R&D project led to the full development and characterization of this new radiopure neutron tagging material. The technology is robust and based on the use of ingredients fully available on the market. The procedure, validated at the industrial level and suitable for the production of large-scale amount of material, has been patented in Italy (Patent for industrial invention n. 102021000028130, classification C08F) and is in the final stages of evaluation for patenting in the USA, EU and China [34].

A   Nanoparticle distribution uniformity measurements

Tab. 10 shows the results of the calcination characterization (reported in Sec. 5.3) on some laboratory samples. These samples were obtained using the same procedure (illustrated in Sec. 4), and differ in thickness (from ≈3 cm to ≈20 cm) and in the concentration of Gd_2O_3 nano-grains. For all, the homogeneity of the distribution of nano-grains along the vertical axis is satisfactory with respect to the requirements of Tab. 1.

Sample	Section	Nominal Gd_2O_3 concentration [$\%_w$]	Measured Gd_2O_3 concentration [$\%_w$]	Surfactant concentration [$\%_w$]
09-06-1	Section 1	1	1.491 ± 0.003	1
	Section 2	1	1.185 ± 0.003	1
19-05-2	Section 1	1	1.115 ± 0.003	1
	Section 2	1	0.914 ± 0.003	1
	Section 3	1	1.503 ± 0.003	1
20-05-1	Section 1	1	0.979 ± 0.003	1
	Section 2	1	0.855 ± 0.003	1
	Section 3	1	1.288 ± 0.003	1
13-10-1	Section 1	2.3	2.662 ± 0.003	2
	Section 2	2.3	2.585 ± 0.004	2
	Section 3	2.3	2.624 ± 0.003	2
	Section 4	2.3	2.570 ± 0.003	2
	Section 5	2.3	1.453 ± 0.003	2
03-11-1	Section 1	1	1.076 ± 0.003	0.1
	Section 2	1	1.308 ± 0.003	0.1
05-10-1	Section 1	2.3	3.007 ± 0.003	2
	Section 2	2.3	2.649 ± 0.002	2
	Section 3	2.3	2.423 ± 0.003	2
	Section 4	2.3	2.501 ± 0.007	2
29-09-1	Section 1	1	1.278 ± 0.002	1
	Section 2	1	1.246 ± 0.003	1
	Section 3	1	1.243 ± 0.003	1
	Section 4	1	1.165 ± 0.003	1
26-05-1	Section 1	1	1.070 ± 0.003	1
	Section 2	1	0.995 ± 0.002	1
	Section 3	1	1.014 ± 0.003	1
	Section 4	1	1.146 ± 0.002	1
09-12-2	Section 1	1	1.104 ± 0.004	0.02
	Section 2	1	0.999 ± 0.004	0.02
	Section 3	1	1,036 ± 0.004	0.02
	Section 4	1	1.029 ± 0.007	0.02

Table 10 continued from previous page

	Section 1	1	1.081 ± 0.002	1
26-05-2	Section 2	1	1.020 ± 0.004	1
	Section 3	1	0.995 ± 0.004	1
	Section 4	1	1.130 ± 0.002	1
	Section 1	1	1.037 ± 0.002	0.1
	Section 2	1	1.132 ± 0.002	0.1
09-12-1	Section 3	1	1.140 ± 0.002	0.1
	Section 4	1	1.266 ± 0.002	0.1
	Section 5	1	1.230 ± 0.003	0.1
	Section 6	1	1.314 ± 0.003	0.1

Table 10: Results of calcination tests carried out on some laboratory samples. It should be noted that the developed procedure allowed us to reach a satisfactory Gd_2O_3 homogeneity for different concentration values of the nano-grains and of the surfactant. Furthermore, the samples shown in the table also differ in thickness, in a range between 3 cm and 20 cm.

References

[1] S. Cebrian er al., [DarkSide Collaboration], "Study of cosmogenic activation above ground for the DarkSide-20k experiment", Astropart. Phys., **152** 102878, (2023)

[2] G. Bertone, D. Hooper, "History of dark matter", Rev. of Mod. Phys. **42** : 44, (2018)

[3] P. Agnes et al., [DarkSide Collaboration], "First results from the DarkSide-50 dark matter experiment at Laboratori Nazionali del Gran Sasso", Phys. Lett. B **743**, 456, (2015)

[4] P. Agnes et al., [DarkSide Collaboration], "Results from the first use of low radioactivity argon in a dark matter search", Phys. Rev. D **93**, 081101, (2016)

[5] P. Agnes et al., [DarkSide Collaboration], "DarkSide-50 532-day dark matter search with low-radioactivity argon", Phys. Rev. D **98**, 102006, (2018)

[6] T. Yano, "Measurement of gamma-ray production from thermal neutron capture on gadolinium for neutrino experiments", Nucl. Instrum. Meth. A **845** 425-428, (2017)

[7] K. Hagiwara et al., "Gamma-ray spectrum from thermal neutron capture on gadolinium-157", Prog. Theor. Exp. Phys., **2** 02, (2019)

[8] S. Agostinelli et al. [GEANT4 Collaboration], "Geant4 – a simulation toolkit", Nucl. Instrum. Meth. A **506**, 250, (2003), https://geant4.web.cern.ch/docs/

[9] International Nuclear Data Committee, "Thermal neutron capture cross sections resonance integrals and G-factors", International Atomic Energy Agency, (2003).

[10] S. F. Mughabghab, "Thermal neutron capture cross- sections: Resonance integrals and g- factors", IAEA Nuclear Data Section, INDC(NDS)–440, (2003)

[11] M.G. Boulay and A. Hime, "Technique for direct detection of weakly interacting massive particles using scintillation time discrimination in liquid argon", Astropart. Phys. **25** 3, (2006)

[12] J. Dobson *et al.*, "Ultra-low background mass spectrometry for rare-event searches", Nucl. Instrum. Meth. A, **879**, 25-30, (2018)

[13] I. Bandac *et al.*, "Ultra-low background and environmental measurements at Laboratorio Subterráneo de Canfranc (LSC)", Appl. Radiat. and Isot. **126**, 127-129, (2017)

[14] M. Laubenstein, "Screening of materials with high purity germanium detectors at the Laboratori Nazionali del Gran Sasso", Int. J. Mod. Phys. A, Volume 32, 1743002, (2017)

[15] P. A. Amaudruz *et al.* [DEAP-3600], "Design and Construction of the DEAP-3600 Dark Matter Detector", Astropart. Phys. **108**, 1-23, (2019)

[16] C. Chuanya *et al.* [JUNO], "A convenient approach to determine U/Th in acrylic to subppt level", (2019), https://indico.cern.ch/event/716552/sessions/310940/attachments/1848752/3040841/A_Convenient_Approach_to_Sub-ppt_Level_Measuring_of_U_and_Th_in_Acrylic.pdf

[17] P.C. Okkerman *et al.*, "Chemical study on alkylphenols", Report by department of Rijkswaterstaat Institute for Coastal and Marine Management (RIKZ), Report: RIKZ/2001.029, (2001) https://edepot.wur.nl/174304

[18] F.C. Nachod and J. Schubert,"Ion Exchange Technology", Academic Press, ISBN 9781483232027, (1956), https://www.sciencedirect.com/science/article/pii/B9781483232027500043

[19] Inamuddin and M. Luqman, "Ion Exchange Technology I", Springer, ISBN 9789400716995, (2012), https://doi.org/10.1007/978-94-007-1700-8

[20] M.E. Ginn et al., "New Columnar and Mixed-Bed Ion Exchange Methods for Surfactant Analysis and Purification", Anal. Chem. **31**, 4, 551–555, (1959), https://doi.org/10.1021/ac50164a028

[21] W. Zhang, "Nanoparticle Aggregation: Principles and Modeling", Nanomaterial: Impacts on Cell Biology and Medicine, Springer (2014), https://doi.org/10.1007/978-94-017-8739-0_2

[22] J. Samuel et al., "Homogeneous dispersion of gadolinium oxide nanoparticles into a non-aqueous-based polymer by two surface treatments", J. Nanopart. Res. **13**, 2417-2428, (2011)

[23] A. Colombo et al., "Nanoparticle-doped large area PMMA plates with controlled optical diffusion", J. Mater. Chem. C **1**, 2927-2934, (2013)

[24] P. R. Griffiths, J. A. De Haseth, "Fourier Transform Infrared Spectrometry", John Wiley & Sons, ISBN: 9780471194040, (2006)

[25] B. J. Berne, R. Pecora, "Dynamic Light Scattering: With Applications to Chemistry, Biology, and Physics", *Dover Publications*, (2002)

[26] E. A. Campo, "Selection of Polymeric Materials", *William Andrew Publishing*, ISBN: 978-0-8155-1551-7, (2008)

[27] S. Affolter, A. Ritter, M. Schmid, "Interlaboratory Tests on Polymers by Differential Scanning Calorimetry (DSC): Determination of Glass Transition Temperature (Tg)", Macromol. Mater. Eng. **286**, 605-610, (2001)

[28] S.W. Kuo et al., "Thermal behavior and specific interaction in high glass transition temperature PMMA copolymer", Polymer **44**, 6873-6882, (2003)

[29] J. E. Mark, "Polymer data handbook", *Oxford Univeristy Press*, ISBN:9780195181012, (2009)

[30] R.J. Brook, "Concise Encyclopedia of Advanced Ceramic Materials", pages 49–51, *Pergamon, Oxford*, doi: 10.1016/B978-0-08-034720-2.50023-X, (1991)

[31] S. Agrawal et al., "Investigation of Thermo-mechanical Properties of PMMA", AIP Conference Proceedings, (2010)

[32] T. A. Osswald et al., "International Plastics Handbook", *Hanser Publishers, Munich*, ISBN: 978-1-56990-399-5, (2006)

[33] Clax s.r.l., https://www.claxitalia.com

[34] Ministero delle imprese e del Made in Italy, https://www.uibm.gov.it/bancadati/Advanced_search/type_url?type=pt&cl=1